INTERNATIONAL JOURNAL FOR NUMERICAL METHODS IN FLUIDS
Int. J. Numer. Meth. Fluids 2002; **39**:1037–1052 (DOI: 10.1002/fld.360)

On streamline diffusion arising in Galerkin FEM with predictor/multi-corrector time integration

Yuzuru Eguchi*,†

Fluid Science Department, Central Research Institute of Electric Power Industry, 1646 Abiko, Abiko-shi, Chiba, 270-1194 Japan

SUMMARY

In the present paper, the author shows that the predictor/multi-corrector (PMC) time integration for the advection–diffusion equations induces numerical diffusivity acting only in the streamline direction, even though the equations are spatially discretized by the conventional Galerkin finite element method (GFEM). The transient 2-D and 3-D advection problems are solved with the PMC scheme using both the GFEM and the streamline upwind/Petrov Galerkin (SUPG) as the spatial discretization methods for comparison. The solutions of the SUPG-PMC turned out to be overly diffusive due to the additional PMC streamline diffusion, while the solutions of the GFEM-PMC were comparatively accurate without significant damping and phase error. A similar tendency was seen also in the quasi-steady solutions to the incompressible viscous flow problems: 2-D driven cavity flow and natural convection in a square cavity. Copyright © 2002 John Wiley & Sons, Ltd.

KEY WORDS: Galerkin formulation; predictor/multi-corrector scheme; streamline diffusion; advection–diffusion problem; cavity flow; comparison with SUPG formulation

1. INTRODUCTION

In the last two decades, intensive efforts have been devoted to the development of stabilized finite element methods to accurately and stably solve the advection–diffusion (AD) problems and/or fluid flow problems. The typical stabilization methods are classified into two families: One is the family of the Galerkin-least squares (GLS) method [1] whose origin can be traced back to the streamline upwind/Petrov Galerkin (SUPG) method proposed by Hughes and Brooks [2]. Actually, the GLS method can be reduced to the original SUPG method, if low order (i.e. linear) interpolation is used for approximation, or if an equation system is hyperbolic [1, 3]. The other family of stabilization methods is the Galerkin method enriched with element-wise bubble functions, which Brezzi *et al.* [4] proved to be equivalent to the SUPG methods under a certain condition. The stabilization methods work well, especially for problems involving unresolvable boundary layers under advection-dominated conditions.

* Correspondence to: Y. Eguchi, Fluid Science Department, Central Research Institute of Electric Power Industry, 1646 Abiko, Abiko-shi, Chiba, 270-1194 Japan.
† E-mail: eguchi@criepi.denken.or.jp

Received 18 June 2001
Revised 6 March 2002

However, the formulations of the above stabilization methods are usually based upon the steady AD equations, eliminating the inertia term as a presupposition.

The question the author would like to raise in this paper is how such elimination of the inertia term can be justified, because the inertia term plays the role of a natural built-in stabilizer, bringing the upwind information downstream with a characteristic advection velocity [5]. In fact, the inertia term and the appropriate time integration induce stabilization effects quite similar to the streamline diffusion of the SUPG formulation. Examples are the forward Euler method supplemented with the balancing tensor diffusivity (BTD) in the Galerkin finite element method (GFEM) [6] and the Taylor–Galerkin method [7].

In the present study, the unsteady AD equations are spatially discretized by the SUPG method (and the GFEM by setting the SUPG parameter τ at zero), and temporally integrated by the predictor/multi-corrector (PMC) scheme. The spatial and temporal formulation is essentially the same as the original SUPG-PMC formulation proposed by Brooks and Hughes [8]. The present author arithmetically shows that the PMC time integration itself possesses a stabilization effect inducing a kind of streamline diffusion, even if the GFEM is employed for the spatial discretization. It is also shown numerically that the GFEM transient solutions of the AD equations are more accurate than the SUPG counterparts, suggesting that the further addition of the streamline PMC diffusion to the SUPG diffusion is too much to yield accurate transient solutions. Similar comparative results are shown for the quasi-steady solutions of incompressible viscous flow problems.

The paper is organized as follows: In Section 2, the basic equations, boundary conditions, spatial and temporal discretization are presented. In Section 3, numerical examples are demonstrated for 2-D and 3-D advection problems as well as 2-D driven and natural convections in a cavity, comparing the GFEM-PMC with the SUPG-PMC. Finally, conclusions are given, suggesting 'Don't stabilize the solutions—they're telling you to put back the annihilated inertia term!' in the same sense as Gresho and Lee [9].

2. THEORY

2.1. Basic equations

The basic equation is the following 3-D advection–diffusion equation with respect to a passive scalar variable, c:

$$\dot{c} + U_j c_{,j} - \kappa c_{,j,j} = s \tag{1}$$

where U_j, κ, and s denote divergence-free velocity field, diffusivity and source, respectively. The superposed dot denotes temporal differentiation, while the subscript comma followed by i, j, or k $(=1,2,3)$ denotes partial differentiation with respect to co-ordinates x_i, x_j or x_k $(=x,y,z)$, respectively. It is assumed that the above equation is supplemented by the following boundary conditions:

$$c = c^{\mathrm{BC}} \quad \text{on } \Gamma_{\mathrm{D}} \tag{2a}$$

$$q = q^{\mathrm{BC}} \quad \text{on } \Gamma_{\mathrm{N}} \tag{2b}$$

The boundaries, Γ_D and Γ_N, do not overlap each other, and cover the whole boundary of the domain. The flux through the boundary, q, is defined as

$$q = \kappa c_{,j} n_j \tag{3}$$

where n_j denotes the outward unit normal vector on the boundary.

2.2. Spatial discretization

In the SUPG method [2, 8, 10], the weighted residual forms for Equation (1), employing $(w_k + \underline{w}_k)$ as the weighting functions, is written as

$$\int_\Omega w_k(\dot{c} + U_j c_{,j} - s)\,\mathrm{d}\Omega + \int_\Omega w_{k,j}\kappa c_{,j}\,\mathrm{d}\Omega + \Sigma_e \int_{\Omega_e} \underline{w}_k(\dot{c} + U_j c_{,j} - \kappa c_{,j,j} - s)\,\mathrm{d}\Omega = \int_{\Gamma_N} w_k q^{BC}\,\mathrm{d}\Gamma \tag{4}$$

For spatial discretization, continuous trial solutions, c, and continuous parts of the weighting functions, w_k, are approximated by $\Phi_\alpha c_\alpha$ and $\Phi_\alpha w_{k\alpha}$ using tri-linear interpolation functions Φ_α at node number α, while the discontinuous parts of the weighting functions, $\underline{w}_k$, are defined as

$$\underline{w}_k = \tau U_j \Phi_{\alpha,j} w_{k\alpha} \quad (= \tau[\mathbf{U}, \boldsymbol{\nabla}] w_k) \tag{5}$$

where $[\,,\,]$ denotes the vector inner product and the intrinsic time scale, τ, is defined on each element as [10]

$$\tau = \frac{\coth(Pe_h) - 1/Pe_h}{\sqrt{[\mathbf{b}, \mathbf{b}]}} \tag{6}$$

Vector $\mathbf{b}$ is defined as $\mathbf{b} = [\mathbf{U}, \boldsymbol{\nabla}]\boldsymbol{\xi}$ where vector $\boldsymbol{\xi}$ denotes the inverse of the geometric mapping from the local co-ordinates $\boldsymbol{\xi} = (\xi, \eta, \zeta)$ to the global co-ordinates $\mathbf{x} = (x, y, z)$, i.e. $\boldsymbol{\xi} = \mathbf{f}^{-1}(\mathbf{x})$. The element Peclet number, Pe_h, is defined with the isotropic diffusivity κ as

$$Pe_h = \frac{[\mathbf{U}, \mathbf{U}]}{\kappa\sqrt{[\mathbf{b}, \mathbf{b}]}} \tag{7}$$

The resulting ordinary differential equations are summarized in the matrix form

$$[\mathbf{M}]\{\dot{\mathbf{c}}\} + [\mathbf{A}]\{\mathbf{c}\} + [\mathbf{D}]\{\mathbf{c}\} = \{\mathbf{s}\} \tag{8}$$

where $[\mathbf{M}]$, $[\mathbf{A}]$ and $[\mathbf{D}]$ denote the consistent mass matrix, the advection matrix, and the diffusion matrix, respectively. The GFEM formulation can be obtained by eliminating the discontinuous weighting functions or by setting τ at zero in the SUPG. In the GFEM, the consistent

mass matrix, the advection matrix, and the diffusion matrix are expressed as

$$\mathbf{M} = A^{\mathrm{e}} \int_{\Omega^{\mathrm{e}}} \Phi_\alpha \Phi_\beta \, \mathrm{d}\Omega \tag{9}$$

$$\begin{aligned} \mathbf{A} &= U_x A^{\mathrm{e}} \int_{\Omega^{\mathrm{e}}} \Phi_\alpha \Phi_{\beta,x} \, \mathrm{d}\Omega + U_y A^{\mathrm{e}} \int_{\Omega^{\mathrm{e}}} \Phi_\alpha \Phi_{\beta,y} \, \mathrm{d}\Omega + U_z A^{\mathrm{e}} \int_{\Omega^{\mathrm{e}}} \Phi_\alpha \Phi_{\beta,z} \, \mathrm{d}\Omega \\ &\equiv U_x \mathbf{A}_x + U_y \mathbf{A}_y + U_z \mathbf{A}_z \end{aligned} \tag{10}$$

$$\begin{aligned} \mathbf{D} &= \kappa A^{\mathrm{e}} \int_{\Omega^{\mathrm{e}}} \Phi_{\alpha,x} \Phi_{\beta,x} \, \mathrm{d}\Omega + \kappa A^{\mathrm{e}} \int_{\Omega^{\mathrm{e}}} \Phi_{\alpha,y} \Phi_{\beta,y} \, \mathrm{d}\Omega + \kappa A^{\mathrm{e}} \int_{\Omega^{\mathrm{e}}} \Phi_{\alpha,z} \Phi_{\beta,z} \, \mathrm{d}\Omega \\ &\equiv \mathbf{D}_{xx} + \mathbf{D}_{yy} + \mathbf{D}_{zz} \end{aligned} \tag{11}$$

where A^{e} stands for the assembly of element matrices, formed on each element domain Ω^{e}, into the global matrix. In Equation (8), vector $\{\mathbf{c}\}$ is composed of unknown nodal values, while vector $\{\mathbf{s}\}$ results from the source term and natural boundary condition (2b). To evaluate these integrals, the discrete Del (Nabla) operator method proposed by Tanahashi and Oki [11] was used to save main memory and computational time.

2.3. Structure of GFEM global matrices

To examine the structure of the global matrices appearing in the GFEM, the matrix components were calculated in the same manner as Eguchi *et al.* [12], assuming a 2-D rectangular mesh evenly spaced by h_x and h_y in x- and y-direction, respectively. Since the variable is interpolated by the bilinear functions on each element, the element matrix is explicitly expressed, for example, as $h_x h_y(1 + \xi_\alpha \xi_\beta/3)(1 + \eta_\alpha \eta_\beta/3)/16$ for the consistent mass matrix appearing in Equation (9), where ξ_α, ξ_β, η_α and η_β are the local nodal co-ordinates, taking $+1$ or -1. Then the element matrices are assembled into the global matrices, and a matrix-by-vector component at the row corresponding to an inner node '0' located at (x_0, y_0) away from the boundary can be arithmetically derived as follows.

Consistent mass:

$$\begin{aligned} [\mathbf{M}]\{\dot{\mathbf{c}}\}_0 = h_x h_y (& 0.25\dot{C}_{-1,1} + 1\dot{C}_{0,1} + 0.25\dot{C}_{1,1} \\ & + 1\dot{C}_{-1,0} + 4\dot{C}_0 + 1\dot{C}_{1,0} \\ & + 0.25\dot{C}_{-1,-1} + 1\dot{C}_{0,-1} + 0.25\dot{C}_{1,-1})/9 \end{aligned} \tag{12}$$

where $C_{m,n}$ is a component of vector $\{\mathbf{c}\}$ and denotes the nodal value at co-ordinates $(x_0 + mh_x, y_0 + nh_y)$. Similarly, the stencils for the lumped mass matrix, the advection matrix and the diffusion matrix in x-direction in the GFEM are calculated as follows:

Lumped mass:

$$[\underline{\mathbf{M}}]\{\dot{\mathbf{c}}\}_0 = h_x h_y \dot{C}_0 \tag{13}$$

Advection in x-direction:

$$U_x[\mathbf{A}_x]\{\mathbf{c}\}_0 = U_x h_x h_y(\begin{array}{lll} -0.25C_{-1,1} & +0C_{0,1} & +0.25C_{1,1} \\ -1C_{-1,0} & +0C_0 & +1C_{1,0} \\ -0.25C_{-1,-1} & +0C_{0,-1} & +0.25C_{1,-1})/3h_x \end{array} \tag{14}$$

Diffusion in x-direction:

$$[\mathbf{D}_{xx}]\{\mathbf{c}\}_0 = \kappa h_x h_y(\begin{array}{lll} -0.5C_{-1,1} & +1C_{0,1} & -0.5C_{1,1} \\ -2C_{-1,0} & +4C_0 & -2C_{1,0} \\ -0.5C_{-1,-1} & +1C_{0,-1} & -0.5C_{1,-1})/3h_x^2 \end{array} \tag{15}$$

It is seen that the weight for C_0 in the 2-D consistent mass is less than half (0.444), while C_0 in the lumped mass is fully weighted, like the mass appearing in the finite difference method (FDM). It is also seen that the stencils of advection and diffusion of GFEM are different from those of the second-order centred FDM (e.g. $U_x(-C_{-1,0}+C_{1,0})/2h_x$ for x-direction advection $U_x c_{,x}$ at a grid '0'), although the stencils of both the GFEM and the FDM coincide under the 1-D condition. This implies that the GFEM solutions, which behave in the same manner as the centred FDM solutions under the 1-D steady condition, can behave differently under multi-dimensional and/or unsteady conditions. This is also true for the relation between the SUPG and the upwind FDM, since these upwind methods converge to the GFEM and the centred FDM in the diffusion limit. On the other hand, the original SUPG formulation is based on the 1-D steady 'optimal' upwind FDM, with which exact solutions can be yielded at each grid or node (i.e. super-convergent solution) [2, 8]. These two facts suggest that the straightforward extension of the SUPG to the multi-dimensional and/or unsteady conditions is quite questionable. The answer is given by numerical examples in Section 3, comparing the multi-dimensional unsteady behaviours computed by the GFEM and the SUPG.

2.4. Predictor/multi-corrector time integration

The PMC scheme is employed in a way identical to the formulation proposed by Brooks and Hughes [8] to temporally integrate the ordinary differential system (8), which is simply rewritten as $\mathbf{Ma} = \mathbf{s} - \mathbf{Kc}$, omitting the parentheses attached to matrix and vector, and defining $\mathbf{a} \equiv \dot{\mathbf{c}}$ and $\mathbf{K} \equiv \mathbf{A} + \mathbf{D}$. Then, the algorithm of the PMC scheme is summarized as

[O] Setup of initial condition

(1) initialize time step number;	$n = 0$
(2) give initial condition of $\mathbf{c}$;	$\mathbf{c}_n = \mathbf{c}_0$
(3) compute initial condition of $\mathbf{a} = \dot{\mathbf{c}}$;	$\mathbf{a}_n = \mathbf{a}_0 = \underline{\mathbf{M}}^{-1}(\mathbf{s} - \mathbf{Kc}_0)$

[I] Predictor phase

(1) reset iteration step counter;	$k = 0$
(2) compute initial guess of $(n+1)$th time step value;	$\mathbf{c}^k = \mathbf{c}_n + \Delta t(1-\gamma)\mathbf{a}_n$
(3) reset $(n+1)$th time step acceleration;	$\mathbf{a}^k = \mathbf{0}$

[II] Multi-corrector phase
(1) compute acceleration increment; $\Delta\mathbf{a}^k = \underline{\mathbf{M}}^{-1}(\mathbf{s} - \mathbf{M}\mathbf{a}^k - \mathbf{K}\mathbf{c}^k)$
(2) update $(n+1)$th time step value; $\mathbf{c}^{k+1} = \mathbf{c}^k + \gamma\Delta t\Delta\mathbf{a}^k$
(3) update $(n+1)$th time step acceleration; $\mathbf{a}^{k+1} = \mathbf{a}^k + \Delta\mathbf{a}^k$
(4) IF $(k+1) < K_{\max}$,

THEN: bump inner iteration step, k, and iterate [II]
ELSE: advance time; $t = t + \Delta t$, $\mathbf{c}_{n+1} = \mathbf{c}^{k+1}$, $\mathbf{a}_{n+1} = \mathbf{a}^{k+1}$,
bump time step, n, and return to [I] (go to next time step)

In the above, $\underline{\mathbf{M}}$ is the lumped mass matrix, $\mathbf{M}$ is the consistent mass matrix, γ is a time integration parameter, and $K_{\max}$ is a prescribed upper limit of the multi-corrector iteration. If $K_{\max} = 1$, the next step value $\mathbf{c}_{n+1}$ is corrected only once in Phase [II], and the one-pass scheme can be written with a single time integration formula as follows:

One-pass scheme:

$$\underline{\mathbf{M}}(\mathbf{c}_{n+1} - \mathbf{c}_n)/\Delta t = (\mathbf{s} - \mathbf{K}\mathbf{c}_n) - \Delta t(1-\gamma)\gamma\mathbf{K}\underline{\mathbf{M}}^{-1}(\mathbf{s} - \mathbf{K}\mathbf{c}_n) + (1-\gamma)(\underline{\mathbf{M}} - \Delta t\gamma\mathbf{K})\{\mathbf{a}_n - \underline{\mathbf{M}}^{-1}(\mathbf{s} - \mathbf{K}\mathbf{c}_n)\} \tag{16}$$

In the one-pass scheme, the consistent mass matrix does not have any effect on the next time step value, because $\mathbf{a}^k = 0$ in Phase [II]. It is expected that the one-pass scheme is inaccurate because of the phase error induced by the mass lumping as explained by Gresho *et al.* [13].

Similarly, the two-pass scheme ($K_{\max} = 2$) is summarized in the following single-equation formula:

Two-pass scheme:

$$\begin{aligned}\underline{\mathbf{M}}(\mathbf{c}_{n+1} - \mathbf{c}_n)/\Delta t = {} & (\mathbf{s} - \mathbf{K}\mathbf{c}_n) - \gamma\Delta t\mathbf{K}\underline{\mathbf{M}}^{-1}(\mathbf{s} - \mathbf{K}\mathbf{c}_n) \\ & + (1-\gamma)\gamma^2\Delta t^2\mathbf{K}\underline{\mathbf{M}}^{-1}\mathbf{K}\underline{\mathbf{M}}^{-1}(\mathbf{s} - \mathbf{K}\mathbf{c}_n) \\ & + \gamma(\mathbf{I} - \mathbf{M}\underline{\mathbf{M}}^{-1})\{\mathbf{I} - (1-\gamma)\Delta t\mathbf{K}\underline{\mathbf{M}}^{-1}\}(\mathbf{s} - \mathbf{K}\mathbf{c}_n) \\ & + (1-\gamma)\underline{\mathbf{M}}\{\mathbf{a}_n - \underline{\mathbf{M}}^{-1}(\mathbf{s} - \mathbf{K}\mathbf{c}_n)\} \\ & + (1-\gamma)\gamma\Delta t(\mathbf{M}\underline{\mathbf{M}}^{-1} - \mathbf{2I} + \gamma\Delta t\mathbf{K}\underline{\mathbf{M}}^{-1}) \\ & \times\mathbf{K}\{\mathbf{a}_n - \underline{\mathbf{M}}^{-1}(\mathbf{s} - \mathbf{K}\mathbf{c}_n)\}\end{aligned} \tag{17}$$

where $\mathbf{I}$ denotes the identity matrix. In the two-pass scheme, consistent mass matrices appear in the fourth and last terms on the right-hand side (RHS) of Equation (17), which are numerically shown to reduce the phase error induced by the mass lumping [8].

2.5. Structure and property of induced matrix

It is seen in Equations (16) and (17) that the PMC scheme induces various terms in addition to the forward Euler term ($\mathbf{s} - \mathbf{K}\mathbf{c}_n$). The most influential one would be the second term on the RHS of Equations (16) and (17). To see the structure and property of the induced term, let us restrict ourselves to the pure advection case without any source on the 2-D rectangular mesh considered in Section 2.3. Then the second term $-\gamma\Delta t\mathbf{K}\underline{\mathbf{M}}^{-1}(\mathbf{s} - \mathbf{K}\mathbf{c}_n)$ can be reduced to $\gamma\Delta t\mathbf{A}\underline{\mathbf{M}}^{-1}\mathbf{A}\mathbf{c}_n$, and the matrix-by-vector component at the row corresponding to the inner node '0' can be calculated as follows, noting $\underline{\mathbf{M}}^{-1}\{\mathbf{c}\}_0 = h_x^{-1}h_y^{-1}\{\mathbf{c}\}_0$ and $\mathbf{A} = U_x\mathbf{A}_x + U_y\mathbf{A}_y$.

$$\mathbf{A}\underline{\mathbf{M}}^{-1}\mathbf{A}\{\mathbf{c}\}_0 = h_x^{-1}h_y^{-1}(U_x^2\mathbf{A}_x^2 + U_xU_y\mathbf{A}_x\mathbf{A}_y + U_xU_y\mathbf{A}_y\mathbf{A}_x + U_y^2\mathbf{A}_y^2)\{\mathbf{c}\}_0 \tag{18}$$

where the components associated with matrices $\mathbf{A}_x^2$, $\mathbf{A}_x\mathbf{A}_y$, $\mathbf{A}_y\mathbf{A}_x$ and $\mathbf{A}_y^2$ have the following structures:

$$\begin{aligned}[\mathbf{A}_x]^2\{\mathbf{c}\}_0 = h_y^2(&1C_{-2,2} + 0C_{-1,2} - 2C_{0,2} + 0C_{1,2} + 1C_{2,2}\\ &+8C_{-2,1} + 0C_{-1,1} - 16C_{0,1} + 0C_{1,1} + 8C_{2,1}\\ &+18C_{-2,0} + 0C_{-1,0} - 36C_0 + 0C_{1,0} + 18C_{2,0}\\ &+8C_{-2,-1} + 0C_{-1,-1} - 16C_{0,-1} + 0C_{1,-1} + 8C_{2,-1}\\ &+1C_{-2,-2} + 0C_{-1,-2} - 2C_{0,-2} + 0C_{1,-2} + 1C_{2,-2})/144\end{aligned} \tag{19}$$

$$\begin{aligned}[\mathbf{A}_x][\mathbf{A}_y]\{\mathbf{c}\}_0 &= [\mathbf{A}_y][\mathbf{A}_x]\{\mathbf{c}\}_0\\ &= h_xh_y(-1C_{-2,2} - 4C_{-1,2} + 0C_{0,2} + 4C_{1,2} + 1C_{2,2}\\ &\quad -4C_{-2,1} - 16C_{-1,1} + 0C_{0,1} + 16C_{1,1} + 4C_{2,1}\\ &\quad +0C_{-2,0} + 0C_{-1,0} + 0C_0 + 0C_{1,0} + 0C_{2,0}\\ &\quad +4C_{-2,-1} + 16C_{-1,-1} + 0C_{0,-1} - 16C_{1,-1} - 4C_{2,-1}\\ &\quad +1C_{-2,-2} + 4C_{-1,-2} + 0C_{0,-2} - 4C_{1,-2} - 1C_{2,-2})/144\end{aligned} \tag{20}$$

$$\begin{aligned}[\mathbf{A}_y]^2\{\mathbf{c}\}_0 = h_x^2(&1C_{-2,2} + 8C_{-1,2} + 18C_{0,2} + 8C_{1,2} + 1C_{2,2}\\ &+0C_{-2,1} + 0C_{-1,1} + 0C_{0,1} + 0C_{1,1} + 0C_{2,1}\\ &-2C_{-2,0} - 16C_{-1,0} - 36C_0 - 16C_{1,0} - 2C_{2,0}\\ &+0C_{-2,-1} + 0C_{-1,-1} + 0C_{0,-1} + 0C_{1,-1} + 0C_{2,-1}\\ &+1C_{-2,-2} + 8C_{-1,-2} + 18C_{0,-2} + 8C_{1,-2} + 1C_{2,-2})/144\end{aligned} \tag{21}$$

If advection is only in x-direction (i.e. $U_y = 0$), then a value proportional to Equation (19) is added in the time integration process. The physical meaning of Equation (19) is the x-direction diffusion, which is computed by the 15 values at $(x_0 - 2h_x, y_0 + nh_y)$, $(x_0, y_0 + nh_y)$ and $(x_0 + 2h_x, y_0 + nh_y)$ in the neighbour of node '0' with $n = -2, -1, 0, 1$ and 2. If the advection is skewed by an angle of θ, let us take new co-ordinates (x', y') where the x' axis is parallel to the advection direction, and define the following rotation matrix $\mathbf{R}$:

$$\mathbf{R} = \begin{pmatrix} \cos\theta\mathbf{I} & -\sin\theta\mathbf{I} \\ \sin\theta\mathbf{I} & \cos\theta\mathbf{I} \end{pmatrix} \tag{22}$$

where $\mathbf{I}$ denotes the identity matrix whose dimension is equal to the number of nodes. Then the uniform advection vector observed in the new co-ordinates, $(U_{x'}\mathbf{e}\ \ \mathbf{0})^{\mathrm{T}}$, is related to the original one, $(U_x\mathbf{e}\ \ U_y\mathbf{e})^{\mathrm{T}}$, with the rotation matrix $\mathbf{R}$ as follows, with $\mathbf{e} = (1\ \ 1\ \ \cdots\ \ 1)^{\mathrm{T}}$ and $\mathbf{0} = (0\ \ 0\ \ \cdots 0)^{\mathrm{T}}$.

$$(U_x\mathbf{e} \quad U_y\mathbf{e})^{\mathrm{T}} = \mathbf{R}(U_{x'}\mathbf{e} \quad \mathbf{0})^{\mathrm{T}} \tag{23}$$

Therefore, the induced term $\mathbf{A}\underline{\mathbf{M}}^{-1}\mathbf{A}\{\mathbf{c}\}_0$ is expressed as follows, using the above relation and noting $\underline{\mathbf{M}}^{-1}\{\mathbf{c}\}_0 = h_x^{-1}h_y^{-1}\{\mathbf{c}\}_0$ and $\mathbf{A} = U_x\mathbf{A}_x + U_y\mathbf{A}_y$.

$$\begin{aligned}
\mathbf{A}\underline{\mathbf{M}}^{-1}\mathbf{A}\{\mathbf{c}\}_0 &= h_x^{-1}h_y^{-1}(U_x\mathbf{A}_x + U_y\mathbf{A}_y)^2\{\mathbf{c}\}_0 \\
&= h_x^{-1}h_y^{-1}(\mathbf{A}_x \quad \mathbf{A}_y)\begin{pmatrix} U_x\mathbf{I} \\ U_y\mathbf{I} \end{pmatrix}(U_x\mathbf{I} \quad U_y\mathbf{I})\begin{pmatrix} \mathbf{A}_x \\ \mathbf{A}_y \end{pmatrix}\{\mathbf{c}\}_0 \\
&= h_x^{-1}h_y^{-1}(\mathbf{A}_x \quad \mathbf{A}_y)\mathbf{R}\begin{pmatrix} U_{x'}\mathbf{I} \\ \mathbf{O} \end{pmatrix}(U_{x'}\mathbf{I} \quad \mathbf{O})\mathbf{R}^{\mathbf{T}}\begin{pmatrix} \mathbf{A}_x \\ \mathbf{A}_y \end{pmatrix}\{\mathbf{c}\}_0 \\
&= h_x^{-1}h_y^{-1}(\mathbf{A}_{x'} \quad \mathbf{A}_{y'})\begin{pmatrix} U_{x'}^2\mathbf{I} & \mathbf{O} \\ \mathbf{O} & \mathbf{O} \end{pmatrix}\begin{pmatrix} \mathbf{A}_{x'} \\ \mathbf{A}_{y'} \end{pmatrix}\{\mathbf{c}\}_0
\end{aligned} \tag{24}$$

where $\mathbf{O}$ is the zero matrix and $(\mathbf{A}_{x'}\ \ \mathbf{A}_{y'})$ is the advection matrix computed in the new co-ordinates system which is related to the original advection matrix $(\mathbf{A}_x\ \ \mathbf{A}_y)$ as follows (see Eguchi *et al.* [12] for proof, taking $\vartheta = -\theta$ in the paper):

$$(\mathbf{A}_{x'} \quad \mathbf{A}_{y'}) = (\mathbf{A}_x \quad \mathbf{A}_y)\mathbf{R} = (\cos\theta\mathbf{A}_x + \sin\theta\mathbf{A}_y, -\sin\theta\mathbf{A}_x + \cos\theta\mathbf{A}_y) \tag{25}$$

Equation (24) suggests that the induced matrix $\mathbf{A}\underline{\mathbf{M}}^{-1}\mathbf{A}$ represents the diffusion acting only in $\pm x'$-direction (or streamline direction) without crosswind diffusion. Then the PMC streamline diffusion is similar to the effect of the SUPG in such a sense, but has a different structure.

3. NUMERICAL EXPERIMENTS

3.1. Stability of the PMC scheme

In order to see the effects of the time integration parameters, γ and Δt, on the numerical stability, the rotating cone problem is solved by the PMC (two pass) scheme with the GFEM and the SUPG. The computational domain is a circular disc with radius of $\sqrt{2}$, which is divided into 50×50 finite elements. A fixed velocity field of anticlockwise rigid rotation is given by defining $(U_x, U_y) = (-y, x)$, while the diffusivity is negligibly small ($\kappa = 10^{-12}$). The initial condition and the boundary condition are given as follows.

$$\textit{Initial condition}: \; c = 0 \quad \text{if } r > 0.4 \text{ where } r^2 = (x - 0.6)^2 + y^2$$
$$c = 0.5(1 + \cos \pi r / 0.4) \quad \text{otherwise}$$
$$\textit{Boundary condition}: \; c = 0 \quad \text{on the whole boundary}$$

Figure 1 shows the maximum and minimum values of c in the domain after one revolution in variation with the parameter γ while fixing Δt at 0.005. The maximum Courant number is estimated around 0.455 at the smallest mesh on the disc periphery where the advection velocity is largest. Figure 2 shows the similar figure as the function of the time

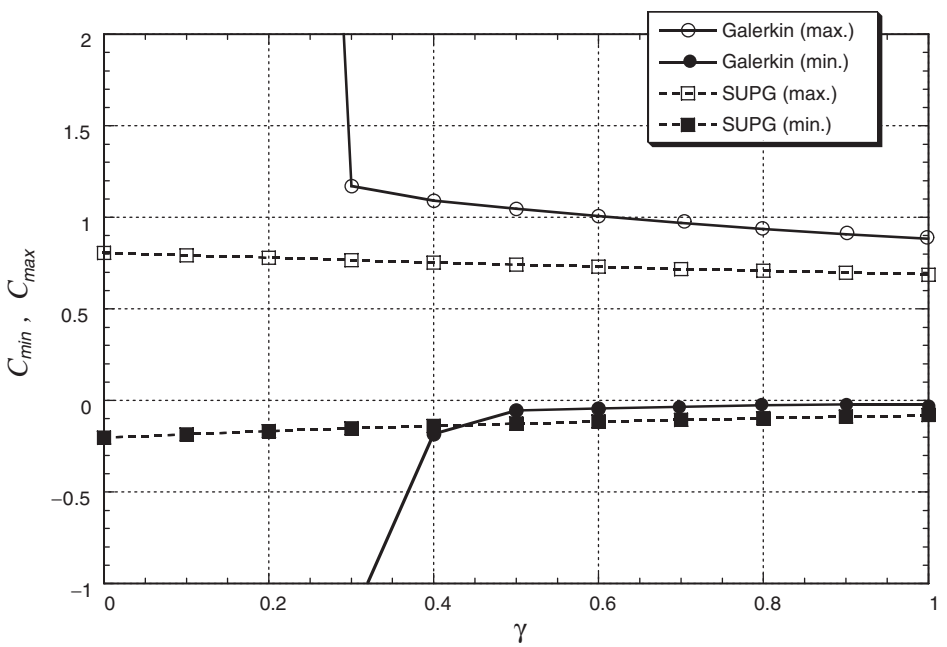

Figure 1. Effect of time integration parameter in the PMC scheme ($\Delta t = 0.005$).

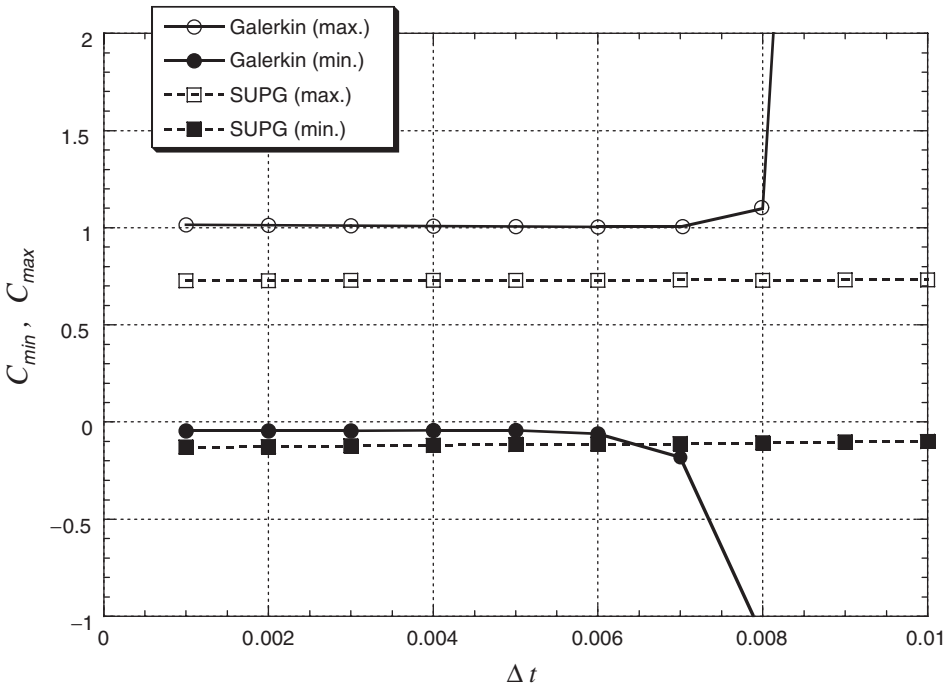

Figure 2. Effect of time increment in the PMC scheme ($\gamma = 0.6$).

increment Δt with fixing γ at 0.6, because the GFEM-PMC solution around $\gamma = 0.6$ is most accurate in Figure 1. These figures show that the SUPG solutions are rather insensitive to the parameters, while the GFEM solutions become unstable under large-Δt or small-γ conditions. However, the GFEM solutions seem more accurate than the SUPG solutions as far as the GFEM solutions are stable, since $c_{\max} = 1$ and $c_{\min} = 0$ for the exact solution.

3.2. *Accuracy*

The accuracy of the spatial discretization and the time integration is numerically examined with the above rotating cone problem among the following explicit schemes:

(i) GFEM-PMC: present formulation with GFEM (one pass/two pass, $\gamma = 0.6$).
(ii) SUPG-PMC: present formulation with SUPG (one pass/two pass, $\gamma = 0.6$).
(iii) FE-BTD: forward Euler method with GFEM and balancing tensor diffusivity [6].
(iv) AB2: second-order Adams–Bashforth method with GFEM.
(v) AB3: third-order Adams–Bashforth method with GFEM.

The mass matrix is lumped in all the schemes whenever the inversion is required and the time increment is fixed at $\Delta t = 0.005$ for all computations. Then, the average Courant number is estimated at 0.06 based on average mesh width and velocity at the initial cone center. Figures 3(a)–3(f) show the terminal results after one revolution, computed by the GFEM-PMC (one pass), the GFEM-PMC (two pass), the SUPG-PMC (one pass), the SUPG-PMC

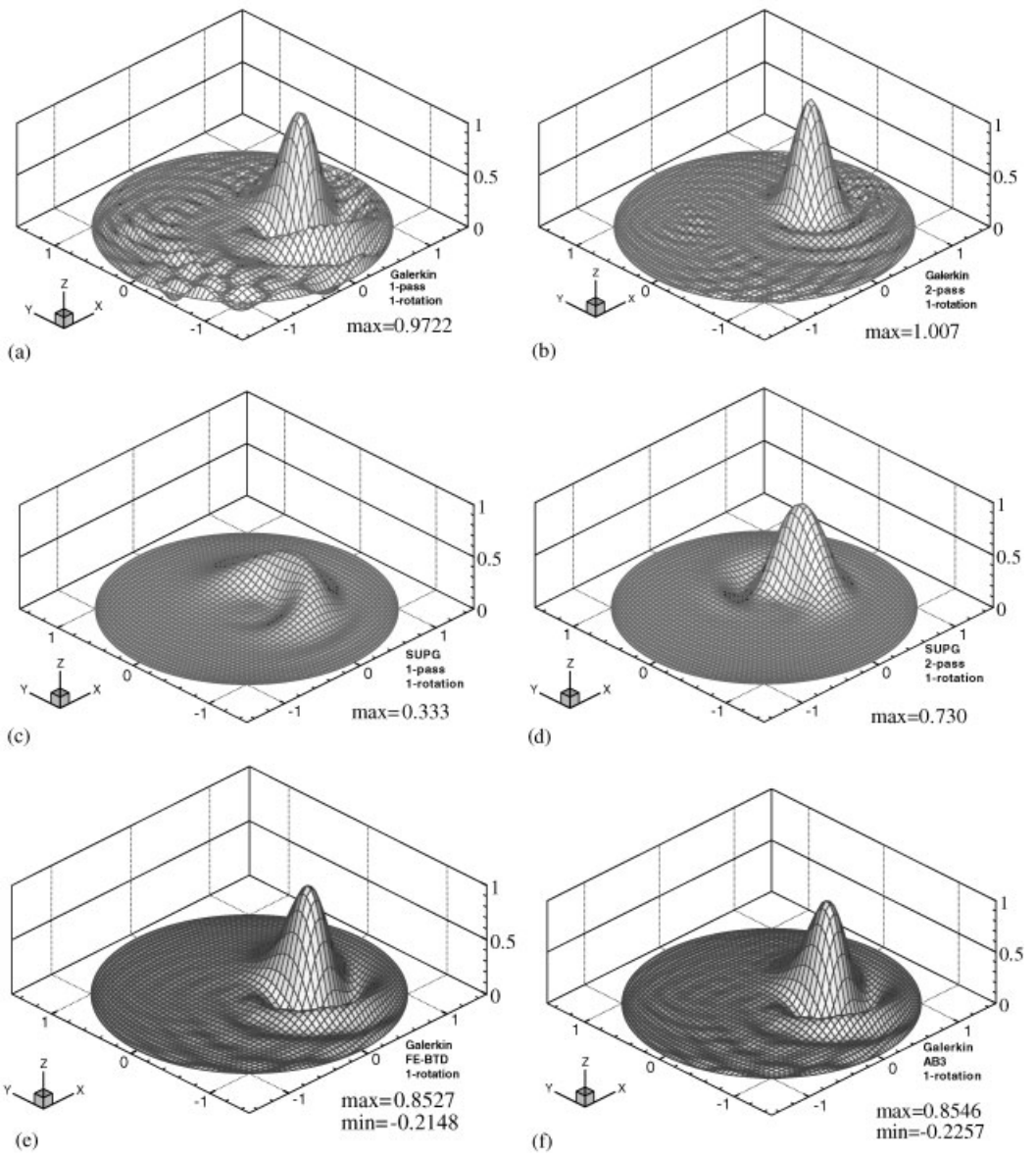

Figure 3. Bird's eye view of cone elevation after one revolution: (a) Galerkin-PMC (one pass) scheme; (b) Galerkin-PMC (two pass) scheme; (c) SUPG-PMC (one pass) scheme; (d) SUPG-PMC (two pass) scheme; (e) forward Euler with BTD scheme; and (f) third-order Adams–Bashforth scheme.

(two-pass scheme), the FE-BTD and the AB3, respectively. Table I quantitatively shows the maximum and minimum values of c and the phase errors after one revolution. The results indicate the superiority of the GFEM-PMC (two pass) to the other schemes in terms of the damping properties and phase error, while the SUPG solutions are damped most.

Table I. Maximum and minimum values of c, and the peak position (phase errors) after one revolution.

Schemes	Quantities		
	Max. value (exact = 1)	Min. value (exact = 0)	Peak position (exact = 0°)
GFEM-PMC (one pass)	0.9722	−0.3887	−21° (lag)
GFEM-PMC (two pass)	1.007	−0.0431	0°
SUPG-PMC (one pass)	0.3328	−0.0168	−11° (lag)
SUPG-PMC (two pass)	0.7296	−0.1157	+11° (advance)
Forward Euler + BTD*	0.8527	−0.2148	−16° (lag)
Second-order Adams–Bashforth	0.8550	−0.2250	−16° (lag)
Third-order Adams–Bashforth	0.8546	−0.2257	−16° (lag)

*BTD: balancing tensor diffusivity.

3.3. 3-D rotating ball problem

Similarly, the rotating ball problem in 3-D space is solved with the PMC (two pass) using the GFEM and the SUPG for spatial discretization. The computational domain is a sphere with radius $\sqrt{3}$, which is divided into $40 \times 40 \times 40$ finite elements. The velocity field of rigid rotation is given by defining $(U_x, U_y, U_z) = (-y, x, 0)$, while the diffusivity is negligibly small ($\kappa = 10^{-12}$). The initial condition and the boundary condition are given by

$$\textit{Initial condition}: \; c = 0 \quad \text{if } r > 0.5 \text{ where } r^2 = (x - 0.75)^2 + y^2 + z^2$$

$$c = 0.5(1 + \cos \pi r / 0.5) \quad \text{otherwise}$$

$$\textit{Boundary condition}: \; c = 0 \quad \text{on whole boundary}$$

The time integration was performed with $\gamma = 0.6$ and $\Delta t = 0.005$, until $t = 3.14$ (half-revolution). The average Courant number is estimated at 0.054 based on the average mesh width and the velocity at the initial ball center. Figures 4(a) and 4(b) show the iso-value surface of $c = 0.1$ of the terminal results computed by the GFEM-PMC (two pass) and the SUPG-PMC (two pass), respectively. The peak value of c and the phase error of the GFEM are 1.028 and 0°, respectively, while those of the SUPG are 0.772 and 6.34° (advance).

3.4. Driven cavity flow

The GFEM-PMC and the SUPG-PMC schemes for the advection–diffusion equation can be extended to the unsteady Navier–Stokes equation to solve the fluid flow problem. The PMC algorithm for incompressible viscous fluid flow problem is shown in the author's preceding paper [14]. The 2-D driven cavity flow problem was solved by the GFEM-PMC (two pass) and the SUPG-PMC (two pass) using a 3-D slab model of $1 \times 50 \times 50$ finite elements. The upper lid, including the corners (i.e. 'leaky' lid), is driven at the velocity of unity, while the other three walls are assumed as non-slip boundaries. The kinematic viscosity of fluid, ν, is varied in the range 0.01–0.0002 to set the Re number at 100–5000. Figures 5(a) and 5(b) show the contours of the stream function of the quasi-steady results ($Re = 1000$) computed

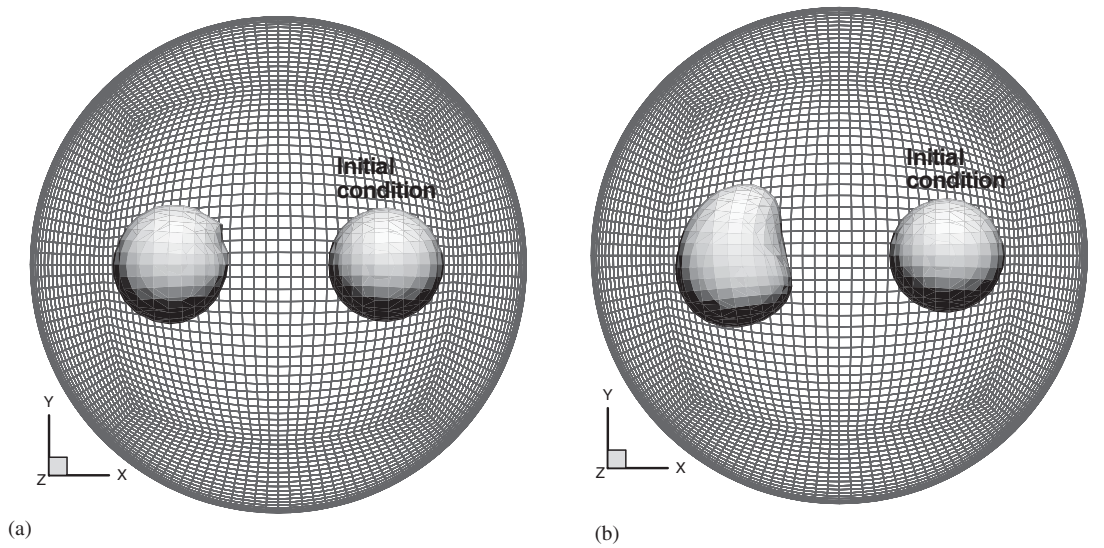

Figure 4. Iso-value ($c = 0.1$) surface after half-revolution of ball computed by PMC (two pass) scheme: (a) Galerkin method; and (b) SUPG method.

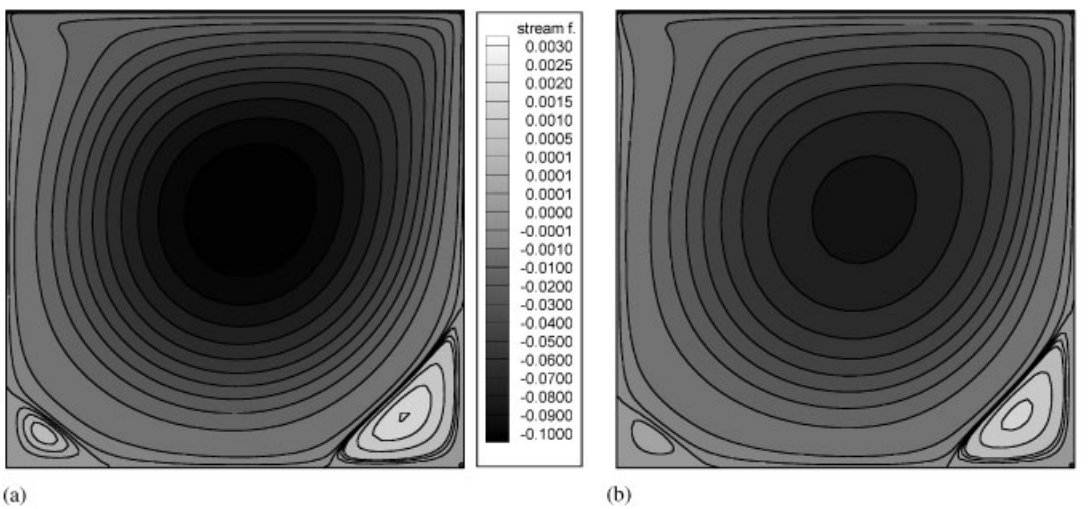

Figure 5. Quasi-steady stream functions of driven cavity flow ($Re = 1000$) computed by PMC (two pass) scheme: (a) Galerkin method; and (b) SUPG method.

by the GFEM and the SUPG, respectively. It is seen that the intensity of the primary center vortex is weaker in the SUPG solution than that of the GFEM, and so are the secondary and third corner vortices. Figure 6 shows the absolute values of the minimum stream function at the primary vortex center in variation with the *Re* number, comparing with the reference

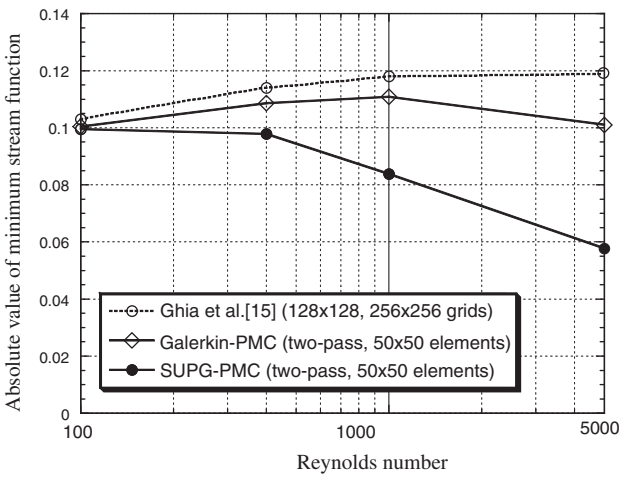

Figure 6. Absolute value of minimum stream function as a function of *Re* number.

solution given by Ghia *et al.* [15]. It can be seen that the SUPG solutions deviate from the reference solutions more than the GFEM solutions as the *Re* number increases, though all the solutions agree well at low *Re* number.

3.5. Thermal cavity flow

The 2-D natural convection in a bi-unit square cavity was similarly solved by the GFEM-PMC and the SUPG-PMC, using a 3-D slab model of $1 \times 40 \times 40$ finite elements. Figures 7(a) and 7(b) show the contours of the non-dimensional stream function, Ψ, in the quasi-steady state for the case of $Pr = 0.71$ and $Ra = 10^6$. The non-dimensional numbers, i.e. Prandtl number, Rayleigh number and Grashof number, are defined as $Pr = \nu/\alpha$, $Ra = Pr\,Gr$, $Gr = UL/\nu$ where α, U and L are thermal diffusivity, representative velocity and the cavity height (or width), respectively. In the present case, the representative velocity U is defined as $g\beta\Delta TL^2/\nu$, where g is the gravitational acceleration; β is thermal expansion coefficient; and ΔT is the temperature difference between the hot and cold walls. It can be seen in the figure that the GFEM solution exhibits the center symmetry, whereas the SUPG solution does not. The quantitative comparison is summarized in Table II with the reference solution given by Comini *et al.* [16]. It is seen that the solution of the GFEM agrees better with the reference solution than that of the SUPG.

4. CONCLUSION

In the present paper, the author has arithmetically derived the streamline diffusion term induced during the predictor/multi-corrector (PMC) time integration even though the centred spatial discretization was employed for the advection–diffusion (AD) equations. This suggests that the inertia term and the time integration itself can play a role of a sort of 'upwind stabilization'. Since the theories of the SUPG and other stabilization formulations are usually constructed

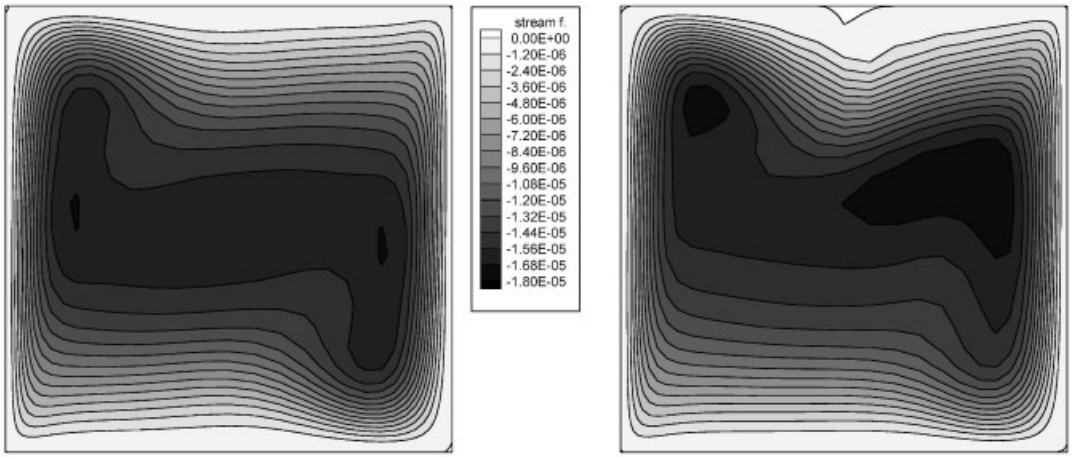

Figure 7. Quasi-steady stream functions of thermal cavity flow ($Ra = 10^6, Pr = 0.71$) computed by PMC (two pass) scheme: (a) Galerkin method; and (b) SUPG method.

Table II. Quantitative comparison of thermal cavity flow solutions.

Schemes	Quantities			
	Stream function $\lvert\Psi\rvert_{\max}$	Averaged $Nu^{\dagger}$ upper: hot wall lower: cold wall	Max. local Nu upper: hot wall lower: cold wall	Min. local Nu upper: hot wall lower: cold wall
GFEM-PMC	16.87*	8.826	17.51	0.970
(two pass)		8.826	17.51	0.970
SUPG-PMC	17.97*	8.695	17.09	1.109
(two pass)		8.699	17.50	0.939
Comini *et al.* [16]	16.81	8.825	17.40	0.979

*The value is multiplied by $10^6 (= Ra)$ to compare with the reference solution [16] where the representative velocity is defined as α/L.
†For the definition of Nu (Nusselt number on wall), see the reference paper [16].

upon steady AD equations neglecting the inertia term, such formulations do not have the advantage of the built-in stability inherent in the unsteady AD equations. On the other hand, starting with the unsteady AD equations and appropriately integrating in time before or after centred spatial discretization, one can probably obtain reasonably accurate and stable solutions as shown in the GFEM-PMC scheme in the present study as well as in the other schemes proposed previously [5–7].

The present numerical tests demonstrated that the transient solutions for the unsteady AD equations and the quasi-steady solutions for the unsteady incompressible NS equations were overly diffusive or viscous with the SUPG. Thus, an SUPG user should be cautious of the

overall numerical diffusion in solving unsteady problems because his time integrator could add excessive diffusivity to the SUPG diffusivity that is appropriate in quantity only for steady equations. The SUPG method and other stabilization methods seem effective only for problems with unresolvable boundary layers, as the inventor recently has interpreted the stabilization methods as a sort of subgrid scale models [17].

ACKNOWLEDGEMENTS

The author would like to express his gratitude to Prof. G. Yagawa, University of Tokyo, for his encouragement in the present study.

REFERENCES

1. Hughes TJR, Franca LP, Hulbert GM. A new finite element formulation for computational fluid dynamics: VIII. The Galerkin/least square method for advective–diffusive equations. *Computer Methods in Applied Mechanics and Engineering* 1989; **73**:173–189.
2. Hughes TJR, Brooks AN. A multi-dimensional upwind scheme with no crosswind diffusion. In *Finite Element Methods for Convection Dominated Flows*, Hughes TJR (ed.), AMD vol. 34. ASME: New York, 1979; 19–35.
3. Franca LP, Frey SL. Stabilized finite element methods: II. The incompressible Navier–Stokes equations. *Computer Methods in Applied Mechanics and Engineering* 1992; **99**:209–233.
4. Brezzi F, Bristeau M-O, Franca LP, Mallet M, Roge G. A relationship between stabilized finite element methods and the Galerkin method with bubble functions. *Computer Methods in Applied Mechanics and Engineering* 1992; **96**:117–129.
5. Bercovier M, Pironneau O. Characteristics and the finite element method. In *Finite element method flow analysis*: *Proceedings of the Fourth International Symposium on Finite Element Methods in Flow Problems*, Kawai T (ed.), Tokyo, 1982; 67–73.
6. Gresho PM, Chan ST, Lee RL, Upson CD. A modified finite element method for solving the time-dependent, incompressible Navier–Stokes equations. Part 1: theory. *International Journal for Numerical Methods in Fluids* 1984; **4**:557–598.
7. Blank H, Rudgyard M, Wathen A. Stabilized finite element methods for steady incompressible flow. *Computer Methods in Applied Mechanics and Engineering* 1999; **174**:91–105.
8. Brooks AN, Hughes TJR. Streamline upwind/Petrov–Galerkin formulations for convection dominated flows with particular emphasis on the incompressible Navier–Stokes equations. *Computer Methods in Applied Mechanics and Engineering* 1982; **32**:199–259.
9. Gresho PM, Lee RL. Don't suppress the wiggles—they're telling you something!. In *Finite Element Methods for Convection Dominated Flows.* Hughes TJR (ed.), AMD Vol. 34. ASME: New York, 1979; 37–61.
10. Hughes TJR, Mallet M, Mizukami A. A new finite element formulation for computational fluid dynamics: II. Beyond SUPG. *Computer Methods in Applied Mechanics and Engineering* 1986; **54**:341–355.
11. Tanahashi T, Oki Y. New theory for hybrid-upwind technique and discrete Del operator for finite element method. *Computational Fluid Dynamics* 1996; **7**:3–14.
12. Eguchi Y, Yagawa G, Fuchs L. A conjugate-residual-FEM for incompressible viscous flow analysis. *Computer Mechanics* 1988; **3**:59–72.
13. Gresho PM, Lee RL, Sani RL. Advection-dominated flows, with emphasis on the consequences of mass lumping. In *Finite Elements in Fluids.* Gallagher RH *et al.* (eds). Vol. 3. Wiley: New York, 1978; 335–350.
14. Eguchi Y. Practical techniques for a 3-D FEM analysis of incompressible fluid flow contained with slip walls and a downstream tube bundle. *International Journal for Numerical Methods in Fluids* 2001; **37**:279–295.
15. Ghia U, Ghia N, Shin CT. High-Re solutions for incompressible flow using the Navier–Stokes equations and a multi-grid method. *Journal of Computational Physics* 1982; **48**:387–411.
16. Comini G, Cortella G, Manzan M. A streamfunction-vorticity-based finite-element formulation for laminar-convection problems. *Numerical Heat Transfer*, *Part B* 1995; **28**:1–22.
17. Hughes TJR. Multiscale phenomena: Green's functions, the Dirichlet-to-Neumann formulation, subgrid scale models, bubbles and the origin of stabilized methods. *Computer Methods in Applied Mechanics and Engineering* 1995; **127**:387–401.

